ACS Photonics

Letter

Cite This: ACS Photonics 2019, 6, 339−344

pubs.acs.org/journal/apchd5

High Reflection from a One-Dimensional Array of Graphene Nanoribbons

Nathan Zhao,[†] Zhexin Zhao,[‡] Ian A. D. Williamson,[‡] Salim Boutami,[‡,§] Bo Zhao,[‡] and Shanhui Fan*[,‡]

[†]Department of Applied Physics, Stanford University, Stanford, California 94305, United States

[‡]Department of Electrical Engineering, Stanford University, Stanford, California 94305, United States

[§]Université Grenoble Alpes, CEA, LETI, Grenoble, 38054, France

ABSTRACT: We show that up to 90% reflectivity can be achieved by using guided plasmonic resonances in a one-dimensional periodic array of plasmonic nanoribbon. In general, to achieve strong reflection from a guided resonance system requires one to operate in the strongly overcoupled regime where the radiative decay rate dominates over the intrinsic loss rate of the resonances. Using an argument similar to what has been previously used to derive the Chu-Harrington limit for antennas, we show theoretically that there is no intrinsic limit for the radiative decay rate, even when the system has an atomic scale thickness, in contrast to the existence of such limits on antennas. We also show that the current distribution due to plasmonic resonance can be designed to achieve a very high external radiative rate. Our results show that high reflectivity can be achieved in an atomically thin graphene layer, pointing to a new opportunity for creating atomically thin optical devices.

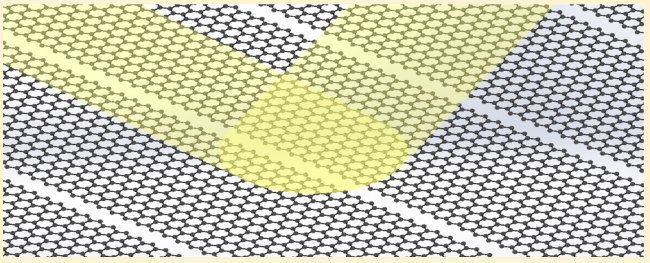

KEYWORDS: *plasmonics, graphene, Chu-Harrington limit, coupled-mode theory*

Recently there has been significant interest in achieving strong reflection from atomically thin materials, with potential applications in high efficiency optical modulators[1] and for achieving large optomechanical interactions.[2] For this purpose, it is essential to create and utilize various kinds of optical resonances in these materials. For example, it has been recently demonstrated that, at low temperature, monolayer $MoSe_2$ can achieve high reflection of incident light due to its excitonic resonance.[1,3] Additionally, the plasmonic resonances of graphene nanoribbons have been studied. Typically, reflection is not the primary point of interest, as the reflectivity is not particularly strong, with values under 20%.[4−7] Related to our work, ref 8 recently observed experimentally radiative rate enhancement in graphene nanoribbon array when the edges of the nanoribbons are brought together. Our work provides a theoretical understanding of this effect and indicates the implication of this effect for reflectivity enhancement.

To achieve strong reflection using a resonance, one must operate in an effectively one-dimensional system where the transmitted and reflected light are restricted to a single diffraction order. Moreover, the resonance must be in the overcoupled regime where the external radiative rate of the resonance dominates over the intrinsic loss rate. Thus, it is important to develop a fundamental understanding of the external radiative rate for a resonance in an effective one-dimensional system. For a resonance in a two- or three-dimensional system, such as the resonance found in an antenna, the Chu-Harrington limit constrains the radiative decay rate with an upper bound proportional to the antenna's physical size.[9−11] However, there has not been a similar understanding of whether there exists a fundamental bound on external radiative decay rate for resonances in effective one-dimensional systems.

In this Letter we theoretically show that there is no upper bound on the radiative decay rate in a one-dimensional resonance. We then demonstrate a practical design approach toward enhancing the radiative decay by engineering the conduction current distribution in a plasmonic resonator consisting of a single-atomic-layer graphene nanoribbons. The resulting structure exhibits high reflection even when realistic loss rates of graphene is taken into account.

To understand the role of a resonance in reflection and the need for a large external radiative rate, consider the exemplary geometry as shown in Figure 1a, where a sheet of graphene nanoribbons is suspended in air with its reflectivity spectrum shown in Figure 1b which exhibits strong reflection. We choose the periodicity, defined as $L = w + d$, to be at subwavelength scale such that for normally incident light the system behaves effectively as a one-dimensional system. Suppose the system supports a resonance. Then, from the temporal coupled mode theory formalism, the reflection of the system has the form[12,13]

Received: November 26, 2018
Published: January 31, 2019

DOI: 10.1021/acsphotonics.8b01640
ACS Photonics 2019, 6, 339−344

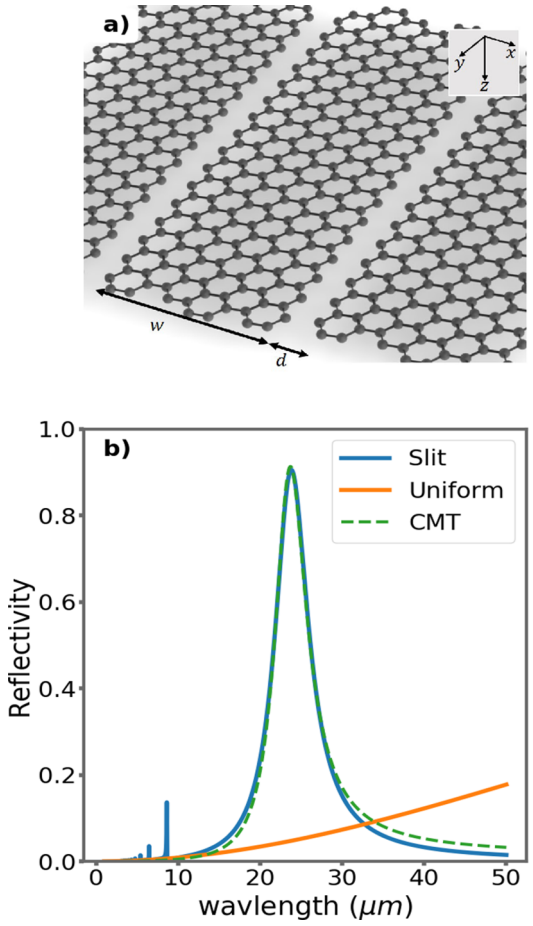

Figure 1. (a) Periodic array of graphene nanoribbons. (b) Numerically computed reflection spectrum for an array of graphene nanoribbons with $w = 0.9\ \mu$m, and $d = 0.050\ \mu$m. The orange line indicates the reflectivity for a single uniform graphene layer and the dashed green line indicates the coupled mode theory (CMT) fit to the 0th order resonance.

$$r(\omega) = e^{j\phi}\left(r_b(\omega) - \gamma_r \frac{r_b(\omega) + jt_b(\omega)}{j(\omega - \omega_0) + \gamma_r + \gamma_i}\right) \tag{1}$$

where ϕ is a phase factor, ω_0 is the resonant frequency, r_b and t_b are the reflection and transmission of the direct scattering process. γ_r represents the external radiative decay rate and γ_i represents the internal loss rate. For extremely thin materials such as graphene operating in the mid- to near-infrared, generally $r_b \approx 0$ and $t_b \approx 1$. From eq 1, high reflectivity requires that the resonance be designed to operate in the overcoupled regime where $\gamma_r \gg \gamma_i$. Therefore, to achieve high reflection it is important to seek to enhance the radiative rate, or equivalently to reduce the quality factor associated with the radiative decay process.

To design a resonance-based reflector with resonant frequency ω_0, it is therefore important to understand any possible constraint on the radiative decay rate. In two- and three-dimensional systems, the radiative decay rate of a resonator is subject to the Chu-Harrington limit. Here we briefly review the arguments of this limit since this understanding is essential for our present work. Related to the radiative decay rate γ_r, one can alternatively define a radiative quality factor, $Q_r = \omega_0/(2\gamma_r)$, which depends on the period-averaged energy stored in the resonator W, as well as the period-averaged radiated power P_{rad} as

$$Q_r = \frac{\omega_0 W}{P_{rad}} \tag{2}$$

Consider a linearly polarized dipole antenna which radiates to free space, and can be bounded by a sphere with radius $r = a$. Assuming that this antenna supports only the TM_{01} mode, then in free space outside the bounding sphere, one of its electric field components has the form:[14]

$$E_\theta \sim e^{-jk_0 r}\left(-\frac{jk_0}{r} - \frac{1}{r^2} + \frac{j}{k_0 r^3}\right) \tag{3}$$

The first term in the parentheses above corresponds to the radiative field, from which one can determine the total radiative power P_{rad} in eq 2. The second and third terms correspond to the nonradiative near-field. Integrating the energy for such near-field component in the volume outside the bounding sphere, we get a lower bound on the stored energy. Therefore, from eq 2, one obtains a lower bound of the radiative quality factor for the dipole antenna,

$$Q_r \geq \frac{1}{k_0 a} + \frac{1}{(k_0 a)^3} \tag{4}$$

While the derivation here is for a dipole antenna, one can in fact show that this bound applies in general for any antenna.[14] A similar derivation can be carried out for two-dimensional systems.[15]

The essence of the derivation above is that in the spherical coordinate system which is appropriate for three dimensions, an outgoing wave in free space always contains near-field components, as shown in eq 3. And hence there is always energy storage associated with such an outgoing wave. Such energy storage necessitates a lower bound in the radiative quality factor. On the other hand, for a one-dimensional system, an outgoing wave solution in free space has the form:

$$E_x(z) \sim e^{-jk|z|} \tag{5}$$

which need not have any near-field component. Thus, using the same argument for the Chu-Harrington limit, as discussed above, one should conclude that there is no limit on the lower bound of the radiative quality factor for a one-dimensional system.

We now show both analytically and numerically that the structure, as shown in Figure 1a, which consists of an array of suspended graphene nanoribbons, provides a pathway to achieve resonances with very high radiative rate. Numerically, we use the Rigorous Coupled Wave Analysis (RCWA) to simulate the structure shown in Figure 1a. We describe the conductivity of graphene as

$$\sigma(\omega) = \frac{2ie^2 k_b T}{\pi\hbar(\omega + i\tau^{-1})}\ln\left[2\cos\left(\frac{\mu}{2k_b T}\right)\right] + \frac{e^2}{4\hbar}\left(G(\omega/2) - \frac{4\omega}{i\pi}\int_0^\infty d\epsilon \frac{G(\epsilon) - G(\omega/2)}{\omega^2 - 4\epsilon^2}\right) \tag{6}$$

where the first term is the intraband term and the second is the interband term and $G(\epsilon) = \sinh(\epsilon/(k_b T))/(\cosh(\mu/(k_b T)) + \sinh(\epsilon/(k_b T)))$, with k_b the Boltzmann constant and T the temperature.[16,17] In eq 6, ϵ is the electron energy (in the conduction band), μ is the chemical potential, and τ is the scattering time. Unless otherwise noted, in this paper, we

DOI: 10.1021/acsphotonics.8b01640
ACS Photonics 2019, 6, 339−344

choose $\mu = 0.8$ eV, $\tau = 1.25 \times 10^{-12}$ s (or an approximate mobility of 10000 $\frac{cm^2}{V \cdot s}$ and carrier density of 5×10^{13} cm^{-2}) to minimize the intrinsic loss while staying close to known experimental results.[18−26] In the RCWA simulation, the graphene sheet is modeled as an effective dielectric layer with a thickness (h) of 0.34 nm with a frequency dependent dielectric constant:[27]

$$\epsilon_r(\omega) = 1 + j\left(\frac{\sigma(\omega)}{\omega \epsilon_0 h}\right) \tag{7}$$

A uniform graphene sheet supports plasmons which are TM-polarized, with the nonzero field components being H_y, E_x, and E_z. In the structure of Figure 1a, the periodicity along the x-direction causes some of these plasmons to radiate into the free space, creating a guided resonance. Here we consider only normally incident light with $k_x = 0$, and choose the periodicity to be below the free space wavelength of light such that the system behaves as an effective one-dimensional system. Since we want to minimize the contribution of nonradiative losses γ_i as that attenuates the reflectivity in eq 1, we operate in the intraband regime where we have strong plasmonic response with low plasmon losses.[28]

For an analytic treatment of the radiative rate γ_r, we must relate the radiated power to specific features of the graphene plasmonic resonator. Such a resonator is described by the surface current density $J_x(x)$. From the surface boundary condition

$$J_x(x) = -[H_y(x, z = 0^+) - H_y(x, z = 0^-)] \tag{8}$$

and Maxwell's equations, we can use $J_x(x)$ to determine the H_y and E_x fields of the resonance. Moreover, the structure in Figure 1a is periodic with mirror symmetry about the center of the nanoribbon at $x = 0$. Therefore, we can decompose the surface current as a Fourier series:

$$J_x(x) = J_x^{(0)} + \sum_{n=1}^{\infty} J_x^{(n)} \cos\left(\frac{2\pi n}{L} x\right) \tag{9}$$

Since the lattice constant is subwavelength, the radiated power P_{rad} is only dependent on the zeroth order Fourier components of E_x and H_y, with all higher order components becoming evanescent and hence nonradiative. Combined with eq 8, we have

$$P_{rad} = \int_{-L/2}^{+L/2} \mathrm{Re}(E_x^{(0)} H_y^{(0)*}) \mathrm{d}x = \frac{L}{4} \sqrt{\frac{\mu_0}{\epsilon_0}} |J_x^{(0)}|^2 \tag{10}$$

Here we take into account that the radiation can go both upward and downward. The higher order, nonradiative components of the Fourier decomposition in eq 9 contribute to the stored energy W, which include both the energy stored in the electromagnetic field as well as in the kinetic energy of the electrons as described in terms of a kinetic inductance.[29] From eq 2, minimizing the Q_r can be framed as maximizing the ratio of P_{rad} to W. With eq 10, we can now see that to minimize the Q_r, one must maximize the relative contribution of $J_x^{(0)}$ compared to the higher order components $J_x^{(n)}$, $n > 0$. In other words, we want to make the contribution of evanescent waves in the stored near field energy as small as possible relative to the radiated power based on eq 2. We thus define the relative contribution of the k^{th} component as

$$R_k = \frac{|J_x^{(k)}|^2 (1 + \delta_{0k})}{\sum_{n=0}^{N} (|J_x^{(n)}|^2 (1 + \delta_{0n}))} \tag{11}$$

where δ_{0k} is the kronecker delta. Equation 11 accounts for the space averaging of the cosine in all the higher order components. The numerically determined surface current distribution $J_x(x)$, for a few nanoribbon array structures, is shown in Figure 2. (The RCWA simulations provide the magnetic field distributions. The surface current distributions are then obtained using eq 8.) A prominent feature of the current distribution is the presence of a kink, that is, a discontinuity in its first derivative, at the edge of the ribbons. This kink, moreover, persists even when the air gap between the ribbon shrinks in size. Such a kink is related to the diverging charge density at the edges of the ribbon. From the charge conservation equation, $\nabla \cdot \mathbf{J} = -i\omega\rho$, within the graphene sheet at its edge, we have $dJ_x/dx \to \infty$, and hence, $dx/dJ_x \to 0$. We can then perform a Taylor expansion of $x(J_x)$ around $x = \pm w/2$ as

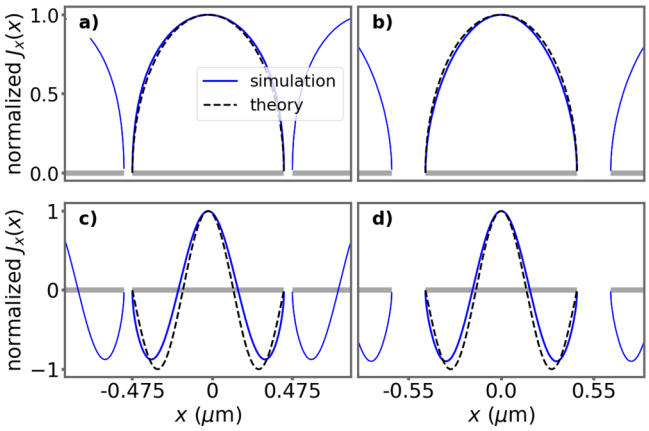

Figure 2. Normalized distributions of the x-component of the current for an array of graphene ribbons with width $w = 0.9$ μm and various gap sizes d. The gray bars represent the graphene nanoribbons: (a) $d = 50$ nm, the lowest order mode; (b) $d = 200$ nm, the lowest order mode; (c) $d = 50$ nm, the second order mode; (d) $d = 200$ nm, the second order mode.

$$x(J_x) \approx \pm\frac{w}{2} + \frac{1}{2}\left(\frac{d^2x}{dJ_x^2}\right) J_x^2 + \ldots \tag{12}$$

Thus, near the edges at $x = \pm w/2$ we have $J_x(x) \sim (x \pm w/2)^{1/2}$. In ref 5, by interpolating the behavior of $J_x(x)$ between two edges, it was argued that $J_x(x)$ has the following form for the lowest order resonance:

$$J_x(x) = \begin{cases} \frac{2}{w}\sqrt{\left(\frac{w}{2}\right)^2 - x^2} & \text{if } |x| \le \frac{w}{2} \\ 0 & \text{if } \frac{w}{2} < |x| < L \end{cases} \tag{13}$$

For our system, eq 13 agrees quite well to the numerically determined current distribution over a wide range of gap sizes shown in Figure 2.

Given $J_x(x)$ in eq 13, we can now decompose it in a Fourier series and analyze how the geometric parameters, d and w, affect the relative contribution of $J_x^{(0)}$. From Figure 3a, the

DOI: 10.1021/acsphotonics.8b01640
ACS Photonics 2019, 6, 339−344

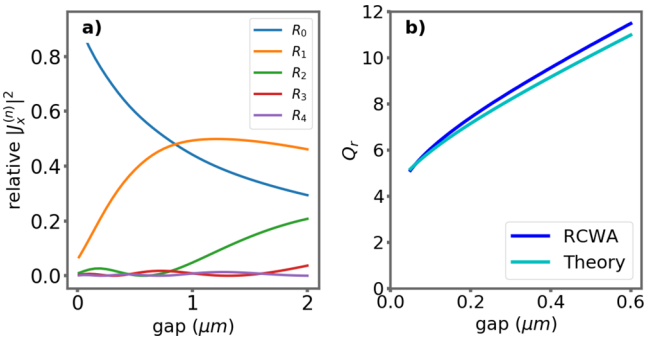

Figure 3. (a) Relative contribution (R_k in eq 11) of the Fourier components of the surface current function $J_x(x)$ in eq 13 as a function of gap size. The systems consist of an array of ribbons with w = 0.90 μm. (b) The cyan curve is the calculated Q_r using the fields derived from the analytic ansatz in eq 13, the blue line is the Q_r determined from our RCWA reflection spectra as fitted using coupled mode theory. The ribbon has a width of w = 0.90 μm.

relative contribution of the zeroth component of $J_x(x)$ increases rapidly with decreasing gap size d for fixed w, while the relative contributions of all the higher order components decrease with decreasing gap size. This clearly indicates that the ratio of the power radiated relative to the power stored is increasing. Consequently, the predicted Q_r, calculated with eqs 2, 8, 9, and 10 decreases with decreasing gap size according to our theory, as shown by the cyan line in Figure 3b.

To support our analysis, we numerically compute the Q_r using the rigorous coupled wave analysis of the same structure. For the same set of structures analyzed in Figure 3b, we simulate their reflection spectra. An exemplary spectrum, for the structure with the width of ribbon w = 0.9 μm and gap size d = 0.050 μm, is shown in Figure 1b. The spectrum features several peaks, and we focus first on the lowest order resonance, which has the longest wavelength, for which the theory as developed above is applicable. To determine its radiative quality factor Q_r, we fit the reflectivity spectrum using eq 1. As shown in Figure 1b, the fit agrees quite well with the numerically determined reflection spectrum. The radiative quality factor Q_r, thus determined for varying gap sizes, is plotted in Figure 3b as the blue line, which agrees quite well with the analytic prediction. Thus, we have indeed shown that very low radiative quality factor, down to the single digits, that is, a very high radiative rate, is achievable in this structure as the gap size reduces. The fit to the reflectivity spectra also determines the intrinsic loss rate Q_i. For the set of structures considered in Figure 3b, $Q_i \approx 100$ is more than an order of magnitude higher than Q_r. Thus, the structures are in the overcoupled regime and exhibits strong reflectivity at resonance. The structure with a gap size of 0.050 μm has a peak reflectivity of 90.5%, as shown in Figure 1b. Thus, we have shown that high reflectivity can be achieved in the graphene nanoribbon array which is atomically thin.

The spectrum in Figure 1b also exhibits narrower peaks at shorter wavelengths that correspond to higher-order resonances. Figure 2c,d shows the current distribution for the second-order resonance. This resonance is the next higher-order resonance that has an even mirror symmetry with respect to the center of the graphene ribbon. Having such an even symmetry is necessary in order for the mode to couple to external radiation from normal incidence. However, the current distribution of this resonance closely resembles a sinusoidal function. Such oscillation of the current distribution for this mode inevitably leads to much larger higher-order Fourier components in eq 9 and hence a much lower radiative rate.

The behavior where the radiative line width increases as the gap size decreases was previously observed experimentally in metallic grating structures[30] but not theoretically explained. While the present focus of the paper is on graphene resonators, our theory also provides a theoretical explanation of the experimental results in ref 30. In general, our theory is applicable to very thin plasmonic systems such as an array of thin metal ribbons. Since we operate graphene in the intraband regime, surface plasmons on a thin metal film will exhibit an approximately similar surface current profile as in eq 13. However, we select graphene as our testbed since it naturally circumvents several issues with plasmonics on ultrathin metal films, namely, that it is difficult to fabricate ultrathin metal films to have a morphologically smooth surface[31−33] and the conductivity of metal films tends to decrease as thickness decreases,[34,35] which would increase material loss and decrease the reflectivity.

Overall, such behavior is unique to plasmonic systems and does not occur in an all-dielectric guided resonance system. As an illustration, in Figure 4 we consider a dielectric grating

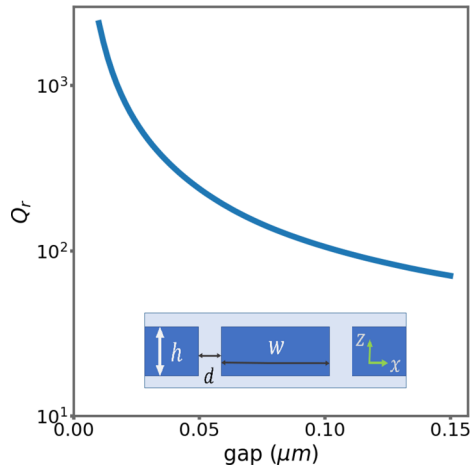

Figure 4. Numerically computed radiative Q-factor for the dielectric grating system. For the dielectric grating (shown in the inset), we use a periodicity along the x-direction of 0.76 μm. The grating has a thickness h = 0.25 μm and a dielectric constant of 3.5. Here, we consider the lowest order guided resonance with a wavelength of approximately 0.96 μm.

structure with a periodic array of air slits introduced into a dielectric slab waveguide. Such a system supports guided resonances.[36] The radiation rate of the guided resonance decreases as the gap sizes decreases since the lateral (x-direction) profile of the guided resonance smoothly approaches that of the guided mode of the dielectric waveguide as the gap size decreases.

Before concluding, we briefly discuss the factors that control the internal loss rate γ_i. Unlike the external radiative decay rate γ_r, which is strongly structure dependent, the internal loss rate γ_i is only weakly dependent on the structural geometry, and is instead mostly controlled by material parameters, such as the chemical potential μ and the scattering time τ in eq 6. These parameters are related to the carrier concentration and the mobility, both of which are more accessible experimentally.

DOI: 10.1021/acsphotonics.8b01640
ACS Photonics 2019, 6, 339−344

The carrier concentration can be tuned via electrostatic gating and doping,[19,37] whereas the mobility can be directly measured. In Figure 5, we show the dependency of the peak

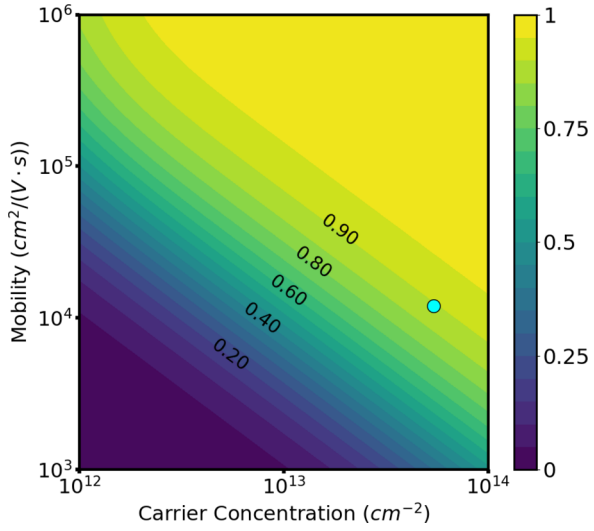

Figure 5. Color map of the peak resonant reflectivity of an array of graphene nanoribbons with w = 0.9 μm and d = 50 nm and varying combinations of mobility and carrier concentration. The cyan dot indicates the set of parameters used for Figure 1b.

reflectivity on carrier concentrations and mobility, for the structure shown in Figure 1b. We see a strong dependency of the reflectivity on these parameters. To achieve high reflectivity generally requires high carrier concentration and high mobility. The choice of the parameters for the spectrum shown in Figure 1b, as indicated by a cyan dot in Figure 5, reflects this requirement, as well as the trade-off between optimizing mobility versus increasing carrier concentration. While the focus of the paper is on single layer graphene, we note that higher mobility and carrier concentrations can be achieved in bilayer or trilayer graphenes,[24,38] which may be more favorable for achieving high reflection.

In conclusion, we have shown that a periodic array of graphene nanoribbon can be designed to achieve high reflectivity. The underlying concept relies upon the general observation of the lack of Chu-Harrington limit in one-dimensional systems and the unique current distribution in very thin 1D plasmonic gratings. By demonstrating this result with graphene, combined with other specific aspects of graphene, such as large in-plane Young's modulus and high melting point, this may open up opportunities for reflectors,[2,39,40] terahertz antennas,[41,42] and potentially light sails.[43]

AUTHOR INFORMATION

Corresponding Author

*E-mail: shanhui@stanford.edu.

ORCID

Nathan Zhao: 0000-0002-2092-6922

Salim Boutami: 0000-0001-6611-5159

Bo Zhao: 0000-0002-3648-6183

Funding

This work is supported by a U.S. AFOSR MURI Project (Grant No. FA9550-17-1-0002).

Notes

The authors declare no competing financial interest.

REFERENCES

(1) Back, P.; Zeytinoglu, S.; Ijaz, A.; Kroner, M.; Imamoglu, A. Realization of an Electrically Tunable Narrow-Bandwidth Atomically Thin Mirror Using Monolayer MoSe 2. *Phys. Rev. Lett.* **2018**, *120*, No. 037401.

(2) Williamson, I. A. D.; Mousavi, S. H.; Wang, Z. Large Cavity-Optomechanical Coupling with Graphene at Infrared and Terahertz Frequencies. *ACS Photonics* **2016**, *3*, 2353−2361.

(3) Scuri, G.; Zhou, Y.; High, A. A.; Wild, D. S.; Shu, C.; De Greve, K.; Jauregui, L. A.; Taniguchi, T.; Watanabe, K.; Kim, P.; Lukin, M. D.; Park, H. Large Excitonic Reflectivity of Monolayer MoSe 2 Encapsulated in Hexagonal Boron Nitride. *Phys. Rev. Lett.* **2018**, *120*, No. 037402.

(4) Ju, L.; Geng, B.; Horng, J.; Girit, C.; Martin, M.; Hao, Z.; Bechtel, H. A.; Liang, X.; Zettl, A.; Shen, Y. R.; Wang, F. Graphene plasmonics for tunable terahertz metamaterials. *Nat. Nanotechnol.* **2011**, *6*, 630−634.

(5) Peres, N. M. R.; Goncalves, P. A. D. *An Introduction to Graphene Plasmonics*; World Scientific, 2013; Chapter 7, pp 163−192.

(6) Yan, H.; Low, T.; Zhu, W.; Wu, Y.; Freitag, M.; Li, X.; Guinea, F.; Avouris, P.; Xia, F. Damping pathways of mid-infrared plasmons in graphene nanostructures. *Nat. Photonics* **2013**, *7*, 394−399.

(7) Strait, J. H.; Nene, P.; Chan, W.-M.; Manolatou, C.; Tiwari, S.; Rana, F.; Kevek, J. W.; McEuen, P. L. Confined plasmons in graphene microstructures: Experiments and theory. *Phys. Rev. B: Condens. Matter Mater. Phys.* **2013**, *87*, 241410.

(8) Semenenko, V.; Schuler, S.; Centeno, A.; Zurutuza, A.; Mueller, T.; Perebeinos, V. PlasmonPlasmon Interactions and Radiative Damping of Graphene Plasmons. *ACS Photonics* **2018**, *5*, 3459−3465.

(9) Wheeler, H. Fundamental Limitations of Small Antennas. *Proc. IRE* **1947**, *35*, 1479−1484.

(10) Chu, L. J. Physical Limitations of OmniDirectional Antennas. *J. Appl. Phys.* **1948**, *19*, 1163−1175.

(11) Harrington, R. F. Effect of Antenna Size on Gain, Bandwidth, and Efficiency. *Journal of Research of NIST* **1960**, *64*, 1−12.

(12) Fan, S.; Suh, W.; Joannopoulos, J. D. Temporal coupled-mode theory for the Fano resonance in optical resonators. *J. Opt. Soc. Am. A* **2003**, *20*, 569.

(13) Haus, H. A. *Waves and Fields in Optoelectronics*; Prentice Hall, 1984.

(14) McLean, J. S. A re-examination of the fundamental limits on the radiation Q of elec- trically small antennas. *IEEE Trans. Antennas Propag.* **1996**, *44*, 672.

(15) Collin, R.; Rothschild, S. Evaluation of antenna Q. *IRE Trans. Antennas Propag.* **1964**, *12*, 23−27.

(16) Falkovsky, L. A. Optical properties of graphene. *Journal of Physics: Conference Series* **2008**, *129*, No. 012004.

(17) Hanson, G. W. Dyadic Green's functions and guided surface waves for a surface conductivity model of graphene. *J. Appl. Phys.* **2008**, *103*, No. 064302.

(18) Gao, W.; Shu, J.; Qiu, C.; Xu, Q. Excitation of Plasmonic Waves in Graphene by Guided-Mode Resonances. *ACS Nano* **2012**, *6*, 7806−7813.

(19) Craciun, M.; Russo, S.; Yamamoto, M.; Tarucha, S. Tuneable electronic properties in graphene. *Nano Today* **2011**, *6*, 42−60.

(20) Bolotin, K.; Sikes, K.; Jiang, Z.; Klima, M.; Fudenberg, G.; Hone, J.; Kim, P.; Stormer, H. Ultrahigh electron mobility in suspended graphene. *Solid State Commun.* **2008**, *146*, 351−355.

(21) Dean, C. R.; Young, A. F.; Meric, I.; Lee, C.; Wang, L.; Sorgenfrei, S.; Watanabe, K.; Taniguchi, T.; Kim, P.; Shepard, K. L.; Hone, J. Boron nitride substrates for high- quality graphene electronics. *Nat. Nanotechnol.* **2010**, *5*, 722−726.

(22) Banszerus, L.; Schmitz, M.; Engels, S.; Dauber, J.; Oellers, M.; Haupt, F.; Watan- abe, K.; Taniguchi, T.; Beschoten, B.; Stampfer, C. Ultrahigh-mobility graphene devices from chemical vapor deposition on reusable copper. *Science Advances* **2015**, *1*, e1500222−e1500222.

(23) Yin, Y.; Cheng, Z.; Wang, L.; Jin, K.; Wang, W. Graphene, a material for high temper- ature devices intrinsic carrier density, carrier drift velocity and lattice energy. *Sci. Rep.* **2015**, *4*, 5758.

DOI: 10.1021/acsphotonics.8b01640
ACS Photonics 2019, 6, 339−344

(24) Ye, J.; Craciun, M. F.; Koshino, M.; Russo, S.; Inoue, S.; Yuan, H.; Shimotani, H.; Morpurgo, A. F.; Iwasa, Y. Accessing the transport properties of graphene and its multilayers at high carrier density. *Proc. Natl. Acad. Sci. U. S. A.* **2011**, *108*, 13002−6.
(25) Efetov, D. K.; Kim, P. Controlling electron-phonon interactions in graphene at ultrahigh carrier densities. *Phys. Rev. Lett.* **2010**, *105*, 256805.
(26) Ni, G. X.; McLeod, A. S.; Sun, Z.; Wang, L.; Xiong, L.; Post, K. W.; Sunku, S. S.; Jiang, B.-Y.; Hone, J.; Dean, C. R.; Fogler, M. M.; Basov, D. N. Fundamental limits to graphene plasmonics. *Nature* **2018**, *557*, 530−533.
(27) Vakil, A.; Engheta, N. Transformation Optics Using Graphene. *Science* **2011**, *332*, 1291−1294.
(28) Jablan, M.; Buljan, H.; Soljaĉić, M. Plasmonics in graphene at infrared frequencies. *Phys. Rev. B: Condens. Matter Mater. Phys.* **2009**, *80*, 245435.
(29) Staffaroni, M.; Conway, J.; Vedantam, S.; Tang, J.; Yablonovitch, E. Circuit analysis in metal-optics. *Photonics and Nanostructures - Fundamentals and Applications* **2012**, *10*, 166−176.
(30) Smythe, E. J.; Cubukcu, E.; Capasso, F. Optical properties of surface plasmon resonances of coupled metallic nanorods. *Opt. Express* **2007**, *15*, 7439.
(31) Malureanu, R.; Lavrinenko, A. Ultra-thin films for plasmonics: a technology overview. *Nanotechnol. Rev.* **2015**, *4*, 259−275.
(32) Yang, X.; Gao, P.; Yang, Z.; Zhu, J.; Huang, F.; Ye, J. Optimizing ultrathin Ag films for high performance oxide-metal-oxide flexible transparent electrodes through surface energy modulation and template-stripping procedures. *Sci. Rep.* **2017**, *7*, 44576.
(33) Bi, Y.-G.; Liu, Y.-F.; Zhang, X.-L.; Yin, D.; Wang, W.-Q.; Feng, J.; Sun, H.-B. Ultrathin Metal Films as the Transparent Electrode in ITO-Free Organic Optoelectronic Devices. *Adv. Opt. Mater.* **2019**, 1800778.
(34) Cottey, A. The electrical conductivity of thin metal films with very smooth surfaces. *Thin Solid Films* **1968**, *1*, 297−307.
(35) Sondheimer, E. H. The mean free path of electrons in metals. *Adv. Phys.* **2001**, *50*, 499−537.
(36) Fan, S.; Joannopoulos, J. D. Analysis of guided resonances in photonic crystal slabs. *Phys. Rev. B: Condens. Matter Mater. Phys.* **2002**, *65*, 235112.
(37) Pachoud, A.; Jaiswal, M.; Ang, P. K.; Loh, K. P.; Özyilmaz, B. Graphene transport at high carrier densities using a polymer electrolyte gate. *EPL (Europhysics Letters)* **2010**, *92*, 27001.
(38) Zhu, W.; Perebeinos, V.; Freitag, M.; Avouris, P. Carrier scattering, mobilities, and electrostatic potential in monolayer, bilayer, and trilayer graphene. *Phys. Rev. B: Condens. Matter Mater. Phys.* **2009**, *80*, 235402.
(39) Sun, K.; Riedel, C. A.; Wang, Y.; Urbani, A.; Simeoni, M.; Mengali, S.; Zalkovskij, M.; Bilenberg, B.; de Groot, C. H.; Muskens, O. L. Metasurface Optical Solar Reflectors Using AZO Transparent Conducting Oxides for Radiative Cooling of Spacecraft. *ACS Photonics* **2018**, *5*, 495−501.
(40) Ginzburg, P.; Krasavin, A. V.; Poddubny, A. N.; Belov, P. A.; Kivshar, Y. S.; Zayats, A. V. Self-Induced Torque in Hyperbolic Metamaterials. *Phys. Rev. Lett.* **2013**, *111*, No. 036804.
(41) Perruisseau-Carrier, J. Graphene for antenna applications: Opportunities and chal- lenges from microwaves to THz. *2012 Loughborough Antennas & Propagation Conference (LAPC)*; IEEE, 2012; pp 1−4.
(42) Zayats, A. V.; Maier, S. A. *Active Plasmonics and Tuneable Plasmonic Metamaterials*; Wiley, 2013; pp 243−261.
(43) Atwater, H. A.; Davoyan, A. R.; Ilic, O.; Jariwala, D.; Sherrott, M. C.; Went, C. M.; Whitney, W. S.; Wong, J. Materials challenges for the Starshot lightsail. *Nat. Mater.* **2018**, *17*, 861−867.

DOI: 10.1021/acsphotonics.8b01640
ACS Photonics 2019, 6, 339−344